

Reliable Entanglement Detection Under Coarse-Grained Measurements

D. S. Tasca,^{1,2} Lukasz Rudnicki,^{3,*} R. M. Gomes,^{2,4} F. Toscano,² and S. P. Walborn²

¹*SUPA, School of Physics and Astronomy, University of Glasgow, Glasgow, G12 8QQ, UK*

²*Instituto de Física, Universidade Federal do Rio de Janeiro,*

Caixa Postal 68528, Rio de Janeiro, RJ 21941-972, Brazil

³*Center for Theoretical Physics, Polish Academy of Sciences, Aleja Lotników 32/46, 02-668 Warsaw, Poland*

⁴*Instituto de Física, Universidade Federal de Goiás, 74.001-970, Goiânia, GO, Brazil*

We derive reliable entanglement witnesses for coarse-grained measurements on continuous variable systems. These witnesses never return a “false positive” for identification of entanglement. We show that, even in the case of Gaussian states, entanglement witnesses based on the Shannon entropy can outperform those based on variances. We apply our results to experimental identification of spatial entanglement of photon pairs.

PACS numbers: 03.67.Mn, 03.65.Ud, 42.50.Xa

Introduction. The detection of quantum entanglement is crucial for the implementation of quantum information tasks and technology. Typically, entanglement is detected through quantum state tomography or the measurement of entanglement witnesses, which involve fewer measurements [1–4]. For continuous variable systems, quantum state tomography is difficult due to the large number of measurements required by the infinite dimensional Hilbert space. Thus, entanglement witnesses are usually more appealing from an experimental point of view. However, even the experimental measurement of an entanglement witness for high-dimensional systems can be very time demanding. This could be due to the large number of measurements required to reconstruct the probability distributions associated to the continuous variables, for example see [5]. It would thus be advantageous to develop entanglement witnesses for coarse-grained measurements. This would allow for faster accumulation of experimental data with acceptable statistics, as well as for the use of less precise detection schemes.

The usual entanglement witnesses for continuous variables can fail under general coarse-grained measurements. In particular, improper application of a CV entanglement witness can result in a “false positive” in the case of extremely coarse-grained measurements. In this paper, using recently derived uncertainty relations [6, 7], we develop new sets of entanglement criteria which are acceptable for measurements with any coarse graining. We illustrate the utility of our approach for spatial variables of entangled photons [8].

Let us consider the Hilbert space $\mathcal{H} = \mathcal{H}_1 \otimes \mathcal{H}_2$ of a continuous bipartite state $\hat{\rho}_{12}$. We have coordinate (x_1, x_2) and momentum (p_1, p_2) variables associated with the corresponding Hilbert spaces. Operators connected with these variables satisfy usual commutation relations: $[\mathbf{x}_k, \mathbf{p}_j] = i\hbar\delta_{kj}$, where $k, j = 1, 2$.

We will consider entanglement witnesses involving the global variables:

$$\mathbf{x}_{\pm} = \mathbf{x}_1 \pm \mathbf{x}_2, \quad \mathbf{p}_{\pm} = \mathbf{p}_1 \pm \mathbf{p}_2, \quad (1)$$

which obey the commutation relations: $[\mathbf{x}_{\pm}, \mathbf{p}_{\pm}] = 2i\hbar$ and $[\mathbf{x}_{\pm}, \mathbf{p}_{\mp}] = 0$. The marginal probability distributions for the bipartite state $\hat{\rho}_{12}$ in the global variables picture (1) read:

$$R_{\pm}(x_{\pm}) = \langle x_{\pm} | \left(\int dx_{\mp} \langle x_{\mp} | \hat{\rho}_{12} | x_{\mp} \rangle \right) | x_{\pm} \rangle, \quad (2a)$$

$$S_{\pm}(p_{\pm}) = \langle p_{\pm} | \left(\int dp_{\mp} \langle p_{\mp} | \hat{\rho}_{12} | p_{\mp} \rangle \right) | p_{\pm} \rangle, \quad (2b)$$

where $|x_{\pm}\rangle$ and $|p_{\pm}\rangle$ are eigenvectors of the operators \mathbf{x}_{\pm} and \mathbf{p}_{\pm} respectively.

A useful entanglement witnesses for continuous variables are the Mancini–Giovannetti–Vitali–Tombsesi (MGVT) criteria [2] which state that if $\hat{\rho}_{12}$ is separable then (from now on we set $\hbar = 1$):

$$\sigma^2[R_{\pm}]\sigma^2[S_{\mp}] \geq 1. \quad (3a)$$

More sensitive tools are the entropic criteria [9] which in the same situation provide the inequality

$$h[R_{\pm}] + h[S_{\mp}] \geq \ln(2\pi e), \quad (3b)$$

that is always stronger than (3a) except for the case of Gaussian states, when both criteria are equivalent. Here the variance $\sigma^2[f]$ and continuous Shannon entropy $h[f]$ of a probability distribution $f(\cdot)$ are defined in the usual manner: $\sigma^2[f] = \int dz z^2 f(z) - (\int dz z f(z))^2$ and $h[f] = -\int dz f(z) \ln[f(z)]$. Since all separable states must satisfy inequalities (3a) and (3b), their experimental violation is an indication of quantum entanglement.

Two couples: (R_+, S_+) and (R_-, S_-) of marginal probability distributions must satisfy the Heisenberg uncertainty relation (HUR) and the Bialynicki-Birula–Mycielski (BBM) uncertainty relation [10], however, with the same lower bounds as those in inequalities (3a) and (3b). Note that these lower bounds differ from the original HUR and BBM by the factor of $4 \equiv 2^2$ and the term $\ln 2$ respectively. This is a consequence of Eq. (1), which describes the transformation $(x_+, x_-) = U(x_1, x_2)$, with $\det U = 2$.

A simple proof of witnesses (3a) and (3b) can be based on the PPT criterion for positive partial transpose [11–13]. If $\hat{\rho}_{12}$ is separable then the operator $\hat{\rho}_{12}^{T_2}$ (the operator $\hat{\rho}_{12}$ transposed with respect to the second Hilbert space \mathcal{H}_2) is positive. Thus, $\hat{\rho}_{12}^{T_2}$ describes a *physical state* so that the HUR and BBM must be satisfied by $(R_{\pm}^{T_2}, S_{\pm}^{T_2})$, as they are satisfied by (R_{\pm}, S_{\pm}) . The partial transposition acts as a mirror reflection in phase space [13], what implies invariance of the marginal position distributions, i.e. $R_{\pm}^{T_2} = R_{\pm}$, while the momentum distributions switch their roles since $S_{\pm}^{T_2} = S_{\mp}$. This observation finalizes the derivation of both separability criteria.

Entanglement witnesses under coarse graining. In practice, an experiment is performed with finite precision. In the case of position and momentum of photons or massive particles this is due to the size of the detector. The experimental results are then discrete random variables which represent the detection probability for each detection position. Let us assume that the continuous distributions are sampled at discrete points and let us introduce the detector function D , which we take to be the rectangle function:

$$D_j^\eta(z) = \begin{cases} 1 & \text{for } z \in [(j - \frac{1}{2})\eta, (j + \frac{1}{2})\eta] \\ 0 & \text{elsewhere} \end{cases}, \quad (4)$$

and define $z_j = j\eta$ so that $D_j^\eta(z)/\eta \rightarrow \delta(z - z_j)$ as $\eta \rightarrow 0$. In position and momentum spaces one shall obtain the detection probabilities $\{r_{\pm}^\Delta\}$ and $\{s_{\pm}^\delta\}$ with values:

$$\{r_{\pm}^\Delta\}_k = \int_{-\infty}^{\infty} dz D_k^\Delta(z) R_{\pm}(z), \quad \{s_{\pm}^\delta\}_l = \int_{-\infty}^{\infty} dz D_l^\delta(z) S_{\pm}(z), \quad (5)$$

related to k th position and l th momentum detectors respectively [14–16]. The variances of these discrete probability distributions can be obtained with [6]:

$$\sigma_{r_{\pm}^\Delta}^2 = \sum_k \{r_{\pm}^\Delta\}_k (x_k^\pm)^2 - \left(\sum_k \{r_{\pm}^\Delta\}_k x_k^\pm \right)^2, \quad (6)$$

and corresponding definitions for momentum variances $\sigma_{s_{\pm}^\delta}^2$. Points $x_k^\pm = k\Delta$ represent centers of the k th detector devoted to measurement of the x_{\pm} variables.

Discrete variances are good approximations to the variances of the continuous distributions (2a) and (2b) if the size Δ (δ) of the detectors is small relative to the probability distributions R_{\pm} (S_{\pm}) [6]. As Δ and δ get large, the variances $\sigma_{r_{\pm}^\Delta}^2$ and $\sigma_{s_{\pm}^\delta}^2$ tend to zero, since most of the continuous distributions R_{\pm} and S_{\pm} will eventually be localized in a single bin. However, the experimentalist is limited by the experimental precision of his/her detectors, which are on the order of Δ and δ . Thus, the variances calculated according to Eq. (6) are not valid

estimators of uncertainty in the general case [6, 7]. When the detectors happen to be too large, this can lead to a false detection of entanglement. For example, consider a pure Gaussian state, with momentum space wavefunction

$$\Psi(p_1, p_2) = A \exp\left(\frac{-(p_1 + p_2)^2}{4\sigma_+^2}\right) \exp\left(\frac{-(p_1 - p_2)^2}{4\sigma_-^2}\right), \quad (7)$$

where A is a normalization constant. For $\sigma_+ = \sigma_-$, the state is separable. Nonetheless, if the size of the bins is about $3\sigma_{\pm}$, the MGVT criteria (3a) can be falsely violated when the variance is calculated according to Eq. (6).

Instead of using the discrete probabilities directly, we can use them to construct approximations to the actual continuous probability distributions for the continuous variables x_{\pm} and p_{\pm} . Let us define the distributions:

$$R_{\pm}^\Delta(x_{\pm}) = \sum_{k=-\infty}^{\infty} \{r_{\pm}^\Delta\}_k \frac{D_k^\Delta(x_{\pm})}{\Delta}, \quad (8a)$$

$$S_{\pm}^\delta(p_{\pm}) = \sum_{l=-\infty}^{\infty} \{s_{\pm}^\delta\}_l \frac{D_l^\delta(p_{\pm})}{\delta}, \quad (8b)$$

so that R_{\pm}^Δ and S_{\pm}^δ go to R_{\pm} and S_{\pm} in the limit $\Delta, \delta \rightarrow 0$. The continuous distributions R_{\pm}^Δ and S_{\pm}^δ are the discretized approximations to R_{\pm} and S_{\pm} obtained through coarse-grained measurements. Figures 2 and 3 show examples of these continuous histogram functions.

Calculating the variances of the distributions (8a) and (8b), one has [6]: $\sigma^2 [R_{\pm}^\Delta] = \sigma_{r_{\pm}^\Delta}^2 + \Delta^2/12$ and $\sigma^2 [S_{\pm}^\delta] = \sigma_{s_{\pm}^\delta}^2 + \delta^2/12$, thus, the discrete variances in general underestimate the inferred variances. As Δ and δ grow large, these variances are given by $\Delta^2/12$ and $\delta^2/12$, which represent the variances of the detector functions.

In a similar fashion, the continuous Shannon entropies of the distributions (8a) and (8b) are [6]:

$$h[R_{\pm}^\Delta] = H[\{r_{\pm}^\Delta\}] + \log \Delta, \quad h[S_{\pm}^\delta] = H[\{s_{\pm}^\delta\}] + \log \delta, \quad (9)$$

where $H[\{r_{\pm}^\Delta\}]$ and $H[\{s_{\pm}^\delta\}]$ are Shannon entropies corresponding to discretizations of the continuous distributions R_{\pm} and S_{\pm} [17], defined by the well known formula $H[\{q\}] = -\sum_k q_k \ln q_k$. In the limit of large Δ, δ the entropies (9) are given by the continuous entropy of the detector function ($\log \Delta$ or $\log \delta$).

Coarse-grained entanglement criteria. Generalizing the uncertainty relation established by Eq. (16) from Ref. [6] (as in the previous case we shall multiply the lower bound by 4), we obtain the inequality

$$\sigma^2 [R_{\pm}^\Delta] \sigma^2 [S_{\pm}^\delta] \geq 1. \quad (10)$$

It has been shown (see an example given by Eqs. (17-19) from [6]) that this relation is not simply a consequence of

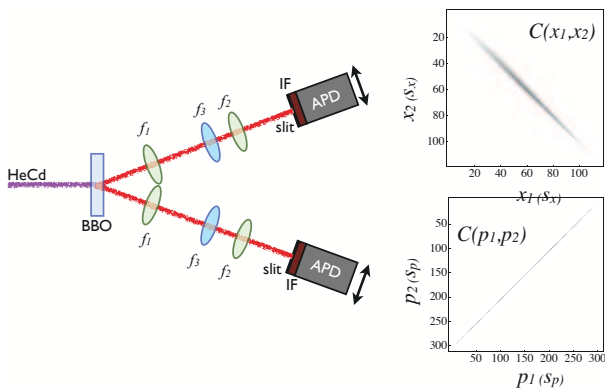


FIG. 1: (color online) Experimental setup (left) and joint coincidence distributions (right). Near- and far-field were mapped onto the detection planes by means of switchable lens systems (see text). The distance from the BBO crystal to the detection planes is 500mm.

the HUR. However, (10) becomes trivially satisfied when $\Delta\delta \geq 12$.

Moreover, we generalize the entropic uncertainty relation given by Eq. (40) from Ref. [7] (according to (1) we shall rescale $\Delta \mapsto \Delta/\sqrt{2}$ and $\delta \mapsto \delta/\sqrt{2}$):

$$H[\{r_{\pm}^{\Delta}\}] + H[\{s_{\pm}^{\delta}\}] \geq -\ln(\Delta\delta) - \ln[\mathcal{C}(\delta\Delta)], \quad (11a)$$

with

$$\mathcal{C}(\gamma) = \min \left\{ \frac{1}{2e\pi}; \frac{1}{4\pi} \left[R_{00} \left(\frac{\gamma}{8}, 1 \right) \right]^2 \right\}. \quad (11b)$$

$R_{00}(\xi, \eta)$ [24] denotes one of the radial prolate spheroidal wave functions of the first kind [18]. The lower bound in (11a) is nonnegative for all values of Δ, δ .

Since R_{\pm}^{Δ} and S_{\pm}^{δ} are linear functionals of R_{\pm} and S_{\pm} we immediately generalize the previous PPT reasoning, i.e. if $\hat{\rho}_{12}$ is separable then:

$$\sigma^2 [R_{\pm}^{\Delta}] \sigma^2 [S_{\pm}^{\delta}] - 1 \geq 0, \quad (12a)$$

$$h[R_{\pm}^{\Delta}] + h[S_{\pm}^{\delta}] + \ln[\mathcal{C}(\delta\Delta)] \geq 0. \quad (12b)$$

Eq. (12a) is an entanglement witness based on the variance product, while Eq. (12b) establishes the entropic entanglement witness, both for the *coarse-grained* probability distributions. In the limit $\Delta \rightarrow 0, \delta \rightarrow 0$ (12a) goes to the MGVT criteria (3a) and (12b) reproduces the entropic criteria (3b). Inequality (12b) is always stronger than (12a) since even for a Gaussian quantum state, the coarse-grained probability distributions, illustrated in Figures 2 and 3, for example, are not Gaussian.

Experiment. We tested the coarse grained entanglement criteria using spatially entangled photons from spontaneous parametric down-conversion (SPDC), prepared approximately in the state (7). A 5mm long BBO

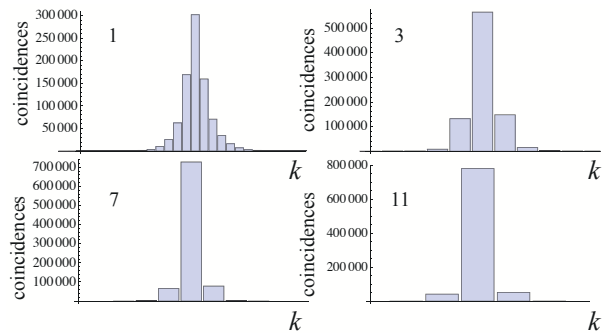


FIG. 2: (color online) Binned histogram distributions for experimental results for x_- measurements for different bin sizes $n = 1, 3, 7, 11$.

crystal was pumped with a 325nm cw pump laser in a TEM00 mode. Down-converted photons at the degenerate wavelength of 650nm were detected through 10nm FWHM interference filters using single photon detectors. For a Gaussian pump beam, the transverse spatial structure of the down-converted photon pairs can be approximately described by a Gaussian wavefunction [8, 19–22], which is factorable in the x and y cartesian coordinates. Within this configuration, we use narrow slits in the detection system to access one of the transverse dimensions of the two-photon field, whose continuous joint detection probability can be estimated from Eq. (7).

As in Ref. [20], the spatial correlations were measured by using optical lens systems to map the near-field (x) and far-field (p) transverse coordinates onto the detection planes. The x measurements used an imaging system with magnification of 4, consisting of a telescope with lenses $f_1 = 50$ mm and $f_2 = 200$ mm, while the p measurements used a Fourier transform system with a lens $f_3 = 250$ mm, as illustrated in Figure 1. We measured two-dimensional arrays of coincidence counts for the near-field (x) and far-field (p) variables by scanning the detectors across the vertical direction in the detection planes. The widths of the slits used in our measurements were $s_x = 0.050$ mm for x measurements and $s_p = 0.020$ mm for p measurements. In both cases, the step size used in the scanning was equal to the slit width (s_x or s_p). The measured joint probability distributions $C(x_1, x_2)$ and $C(p_1, p_2)$ are shown in the right-hand side of Fig. 1. These were then normalized to obtain probability distributions $R(x_1, x_2)$ and $S(p_1, p_2)$.

The marginal distributions $R_{-}^{\Delta_n}$ and $S_{+}^{\delta_m}$ were calculated from the joint distributions in Fig. 1 by grouping the measurements into different size bins $\Delta_n = n\Delta_1$, $\delta_m = m\delta_1$, where $n, m = 1, 3, 5, 7, \dots$. The smallest bin size is $\Delta_1 = 2s_x(f_1/f_2) = 0.0250$ mm and $\delta_1 = 2s_p(2\pi/f_3\lambda) = 1.546$ mm $^{-1}$. Examples of the histogram distributions (before normalization) $R_{-}^{\Delta_n}$ and $S_{+}^{\delta_m}$ are shown in Figures 2 and 3. Figure 4 (a) and (b) shows the entangle-

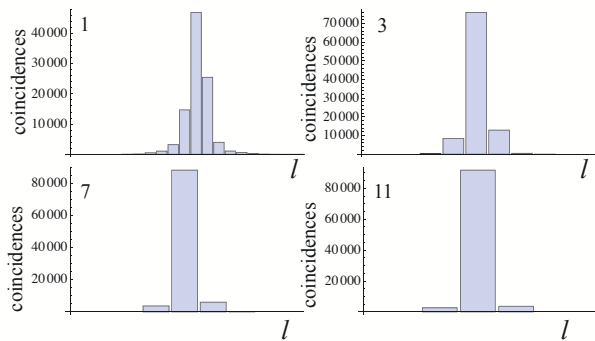


FIG. 3: (color online) Binned histogram distributions for experimental results for p_+ measurements for different bin sizes $m = 1, 3, 7, 11$.

ment witnesses (12a) and (12b) as a function of the number of bin sizes n and m , respectively. The black region shows the area in which the witnesses do not detect entanglement. It can be seen that the entropic criteria identifies entanglement for even larger bins than the variance criteria. This can be seen more distinctly in Figure 4 (c), which shows these same results for the case $n = m$. As can be seen, even for this approximately Gaussian state the entropic criteria outperform the generalized variance product criteria, due to the coarse graining.

Error bars, which are smaller than the symbols in Figure 4 (c), were calculated by propagating the Poissonian counts statistics, as well as the error in the center position of each bin, which we defined to be $\sigma_{\Delta_p} = 0.01\sqrt{2n}f_1/f_2 = 0.004\text{mm}$ and $\sigma_{\delta_m} = 0.01\sqrt{2}(2m\pi/f_3\lambda) = 0.55\text{mm}^{-1}$. Here 0.01mm is the minimum step size of the micrometers used to translate the detectors.

Conclusions Building on previous results for entropic and variance-based uncertainty relations, we have presented entanglement witnesses for continuous variable measurements that are obtained using discretized detection systems. Our results have been tested in an experiment witnessing spatial entanglement in photon pairs obtained from parametric down-conversion. Due to the non-Gaussian nature of the binned histogram distributions inferred from discretized measurements, the entropic entanglement witness performs better than the variance-based witness. These results should be applicable in other continuous variable quantum systems.

Note added: Upon completion of this work, we became aware of similar results obtained by considering Einstein-Podolsky-Rosen-Steering inequalities [23].

We acknowledge financial support from the Brazilian funding agencies CNPq and FAPERJ. This work was performed as part of the Brazilian Instituto Nacional de Ciência e Tecnologia - Informação Quântica (INCT-IQ). This research was also supported by a grant from the Polish Ministry of Science and Higher Education for the

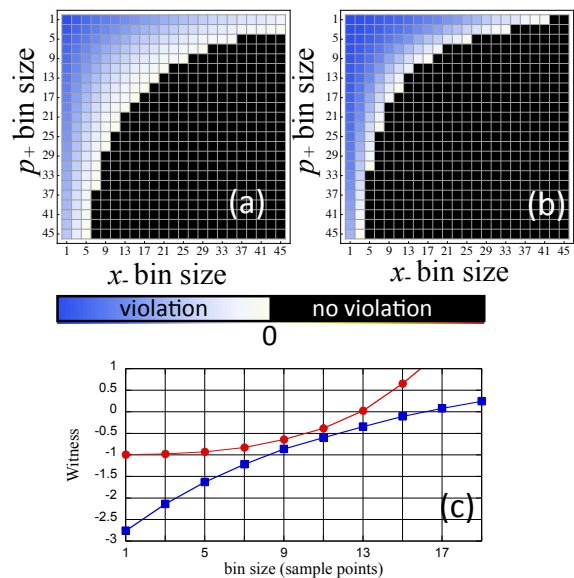


FIG. 4: (color online) Evaluation of entanglement witnesses: (a) Entropic criteria (12b) and (b) Variance criteria (12a) both as a function of the bin size n and m . Black denotes the region where criteria are not violated. (c) Evaluation of entanglement witnesses for the same bin size ($n = m$). The entropic criteria (blue squares) detects entanglement for a larger bin size than the variance criteria (red circles).

years 2010–2012.

* Electronic address: rudnicki@cft.edu.pl

- [1] L.-M. Duan, M. D. Lukin, J. I. Cirac, and P. Zoller, *Nature* **414**, 413 (2001).
- [2] S. Mancini, V. Giovannetti, D. Vitali, and P. Tombesi, *Physical Review Letters* **88**, 120401 (2002).
- [3] R. Horodecki, P. Horodecki, M. Horodecki, and K. Horodecki, *Rev. Mod. Phys.* **81**, 865 (2009).
- [4] O. Gühne and G. Tóth, *Physics Reports* **474**, 1 (2009), ISSN 0370-1573.
- [5] M. Edgar, D. Tasca, F. Izdebski, R. Warburton, J. Leach, M. Agnew, G. Buller, R. Boyd, and M. Padgett, *Nature Communications* **3**, 984 (2012).
- [6] L. Rudnicki, S. P. Walborn, and F. Toscano, *Europhys. Lett* **97**, 38003 (2012).
- [7] L. Rudnicki, S. P. Walborn, and F. Toscano, *Phys. Rev. A* **85**, 042115 (2012).
- [8] S. P. Walborn, C. H. Monken, S. Pádua, and P. H. S. Ribeiro, *Phys. Rep.* **495**, 87 (2010).
- [9] S. P. Walborn, B. G. Taketani, A. Salles, F. Toscano, and R. L. de Matos Filho, *Phys. Rev. Lett.* **103**, 160505 (2009).
- [10] I. Białynicki-Birula and J. Mycielski, *Commun. Math. Phys.* **44**, 129 (1975).
- [11] A. Peres, *Phys. Rev. Lett.* **77**, 1413 (1996).
- [12] P. H. M. Horodecki and R. Horodecki, *Phys. Lett. A* **223**, 1 (1996).
- [13] R. Simon, *Phys. Rev. Lett.* **84**, 2726 (2000).

- [14] I. Bialynicki-Birula, Phys. Lett. **103 A**, 253 (1984).
- [15] I. Bialynicki-Birula, Phys. Rev. A **74**, 052101 (2006).
- [16] I. Bialynicki-Birula and L. Rudnicki, in *Statistical Complexity*, edited by K. D. Sen (Springer, 2011), pp. 1–34.
- [17] Cover and Thomas, *Elements of Information Theory* (John Wiley and Sons, 2006).
- [18] M. Abramowitz and I. Stegun, *Handbook of Mathematical Functions* (Dover, New York, 1964).
- [19] C. H. Monken, P. S. Ribeiro, and S. Pádua, Phys. Rev. A. **57**, 3123 (1998).
- [20] J. C. Howell, R. S. Bennink, S. J. Bentley, and R. W. Boyd, Phys. Rev. Lett. **92**, 210403 (2004).
- [21] C. K. Law and J. H. Eberly, Phys. Rev. Lett. **92**, 127903 (2004).
- [22] D. S. Tasca, S. P. Walborn, P. H. S. Ribeiro, and F. Toscano, Physical Review A **78**, 010304 (2008).
- [23] J. Schneeloch, P. B. Dixon, G. A. Howland, C. J. Broadbent, and J. C. Howell, quant-ph/12104234.
- [24] in the Wolfram Mathematica's notation it reads `SpheroidalS1[0, 0, ξ , η]`.